Enhancing hydrogen production from the pyrolysis-gasification of biomass by size-confined Ni catalysts on acidic MCM-41 supports

Mengjing Ye[a,‡], Yongwen Tao[a,‡], Fangzhu Jin[a], Huajuan Ling[a], Chunfei Wu[c*], Paul T. Williams[b*], Jun Huang[a*]

[a]School of Chemical and Bimolecular Engineering, the University of Sydney, Australia, NSW 2037 (Tel: +61 2 9351 7483; Email: jun.huang@sydney.edu.au)

[b]School of Chemical & Process Engineering, University of Leeds, Leeds LS2 9JT, UK (Tel: +44 113 3432504; Email: p.t.williams@leeds.ac.uk)

[c]School of Chemical Engineering, University of Hull, Hull, HU6 7RX (Tel: +44 1482 466464; Email:C.Wu@hull.ac.uk

‡ Co-first authors.

Abstract: Hydrogen, currently produced from the reforming of fossil fuel resources, is a significant source for clean energy and the chemical industry. It is promising to develop a high-efficiency hydrogen production process from renewable biomass for sustainable development. This research reports that catalyst support acidity could strongly enhance the hydrogen production from the biomass gasification of wood sawdust. For minimizing the influence of the Ni particle size for the biomass gasification, the uniform Ni nanoparticles around 2-3 nm were loaded into one type of mesoporous support MCM-41 with various acidity. Ni/H-[Al] MCM-41 with a large amount of Brϕnsted acid sites contributed 2-3 times higher hydrogen yield (21.6 mmol H_2 g^{-1} sample) than that on Ni/H-[Si]MCM-41 with a small amount of very weak acidic surface SiOH groups (9.8 mmol H_2 g^{-1} sample) and that on nonacidic Ni/Na-[Si]MCM-41 (6.7 mmol H_2 g^{-1} sample). The surface acid sites on supports could generate bifunctional catalysts and were proposed to show two functions for enhancing the hydrogen production: 1) help to crack and transfer the pyrolysis chemicals into smaller compounds for more efficient reforming on the Ni surface inside nanopores; 2) enhance the support and Ni interaction for better reduction property and surface activity of Ni nanoparticles and improve the reforming performance. The obtained Ni/MCM-41 catalysts were quite stable and no sintering has been observed after the gasification at 800 ^oC, and only a low coke deposition has been detected.

Key words: Biomass gasification, hydrogen production, wood sawdust, Ni catalysts, support acidity, MCM-41

1. Introduction

Hydrogen has been increasingly promoted as a clean energy source since its combustion product is only water without any greenhouse gases (GHG) emission. Nowadays, hydrogen is mainly produced from carbon-rich fossil fuel resources such as natural gas, coal, and crude oil, with a significant amount of GHG emissions discharged to atmosphere [1]. To find a renewable resource for hydrogen production, many approaches have been investigated where biomass gasification has provided a very promising option. This is due to the fact that biomass is abundant in nature and it is a CO_2-neutral resource [2]. Catalysts play an essential role to improve the hydrogen production in biomass gasification and Ni-based catalysts have been frequently studied because of their acceptable activity and low cost compared with noble metal catalysts [3-6].

It has been reported from the literature that catalysts with smaller particle size and high dispersion shows higher catalytic activity and lower deactivation [7-10]. Silva et al. [11] suggested that reducing Co particle size (<3nm) decreased the deactivation rate and demonstrated the lower amount of carbon deposition (0.71 mg carbon/mg catalyst) for ethanol steam reforming. Wu et al. [12] reported that NiO particles located inside the MCM-41 mesopores demonstrated higher hydrogen production from biomass gasification and suggested that smaller Ni particles (3nm) inside the MCM-41 mesopores promoted water gas shift reaction and reforming reactions of hydrocarbons and methane due to the longer residence time of reactants inside the MCM-41 pores. Therefore, nano-porous supports are popular for reforming reactions due to its high surface area, well-defined structure for small metal nanoparticles [13-17].

Apart from particle size, the chemical property and surface functional groups of supports also play an important role in the performance of catalysts due to the various reaction pathways by multifunctional groups or support-metal interactions [18, 19]. It should be noted that surface acidity exists on nearly all of current supports, which have a significant effect for reactions [20-26]. Youn et al. [20] investigated Ni catalysts supported on Al_2O_3, MgO, ZrO_2, TiO_2 and ZnO with different surface acidity and reported that $Ni/Ti_{0.2}Zr_{0.8}O_2$ with intermediate acidity of support showed the best catalytic performance for hydrogen production during ethanol reforming. However, Emma et al. [21] reported the Ni catalyst on the acid support showed lower methane conversion compared to that on the neutral

support during methane dry reforming. Therefore, there is still a debate as to whether the acidity of support has positive or negative influence for reactions.

For biomass gasification, the effect from support acidity has not been well investigated. In this paper, we address whether the existence of surface acidity of catalyst supports significantly influences the catalytic performance of the supported metal nanocatalysts in biomass gasification using supported Ni catalysts as an example. One type of support MCM-41 with uniform nano-pores has been applied to size the Ni nanoparticles and minimize the effects from the Ni particle size for the reaction. MCM-41 supports have been synthesized with the acidity (Al form), without acidity (neutral form, may exist as very weak acidic surface OH groups), and without acidity (Na form) [27, 28]. Ni particles could be impregnated into uniform nanopores to realize uniform particle sizes. The obtained Ni/MCM-41catalysts with and without support acidity were investigated for hydrogen production from biomass gasification.

2. Experimental

2.1 Materials

Wood sawdust was used with particle size of less than 0.2 mm with a moisture content of 5.7 wt.%, volatile content of 74.8 wt.%, fixed carbon content of 18.3 wt.% and ash content of 1.2 wt.%.

MCM-41 support was prepared according to the procedure reported by Cheng et al. [29] For H-[Al]-MCM-41 and Na-[Si]-MCM-41 supports, the mole ratio of Al/Si and Si/Na are equal to 1:10 and 1:2 respectively. Calculated amounts of aluminum sulfate and sodium carbonate were added to the MCM-41 materials. The obtained gels were completely mixed with vigorous stirring for 1h. The resulting solids were collected by filtration, washed with distilled water, and then dried in an oven at 80 ^{o}C. Finally, the obtained cake was calcined at 550 ^{o}C with a heating rate of 1 ^{o}C min^{-1} in the presence of static air for 6 h.

Wet impregnation method was used to synthesize catalysts by loading Ni on porous H-[Si]-MCM-41, H-[Al]-MCM-41, Na-[Si]-MCM-41, SiO_2 supports, respectively (The mole

ratio is Ni/Al=1:1). The required amount of Ni $(NO_3)_2.6H_2O$ was dissolved in ethanol to form 1 mol L^{-1} of solution. The impregnation was employed by the addition of powdered H-[Si]-MCM-41, H-[Al]-MCM-41, Na-[Si]-MCM-41, SiO_2 supports to the nickel precursor solution. The mixture was stirred overnight followed by evaporation of the mixture at 80 ^oC. The obtained solids were calcined at 550 ^oC with a heating rate of 1 ^oC min^{-1}, then maintained at 550 ^oC for 6 h in static air.

2.2 Pyrolysis-Gasification of wood sawdust

The biomass gasification experiments were carried out in a two-stage fixed bed reaction system, which has been reported in our previous work [30]. Biomass sawdust was pyrolyzed in the first reactor, the derived gaseous pyrolysis products are passed directly to the second reactor where catalytic steam reforming occurred. For each experiment, about 1.0 g sawdust and 0.5g catalyst were used. Sawdust was placed inside the first reactor, and the catalyst was placed inside the 2^{nd} reactor. Both reactors were separately externally electrically heated. The temperatures of the two reactors were controlled separately using two temperature controllers. Initially, the temperature of the catalyst bed (2^{nd} reactor) was heated and stabilized at 800 °C. Then the first pyrolysis reactor was started to be heated up to 550 °C with a heating rate of 40 °C min^{-1}. Water was injected to the top of the 2^{nd} reactor with a flow rate of 4.74 ml h^{-1} by a syringe pump when the pyrolysis temperature reached around 200 °C. N_2 was used as carrier gas for each experiment with a flow rate of 80 ml min^{-1}. The derived gaseous products after the second reactor were condensed with dry ice cooled condensers to produce the liquid products and the non-condensed gases were collected with a Tedlar gas sample bag for later analysis. It is noted that the whole catalytic reaction time was about 40 mins for each experiment. Selected experiment was repeated to ensure the reliability of the data. Mass balance close to 100% was used as an indicator of an acceptable experiment.

2.3 Products analysis and characterization

The non-condensed gases were analyzed off-line by gas chromatography (GC). The CO_2 gas was analyzed by Varian 3380 GC with a Hysep 80-100 mesh column and argon as carrier gas. CO, H_2, and N_2 gases were determined by another Varian 3380 GC equipped

with a 60-80 mesh molecular sieve column with argon carrier gas. C_1 ─ C_4 hydrocarbons were detected using a further Varian 3380 GC with a flame ionization detector while N_2 is working as carrier gas.

Surface area, average pore size, and total pore volume of the fresh catalysts were determined by N_2 adsorption and desorption isotherms on a Quantachrome Autosorb^{-1}. Each sample (50mg) was degassed at 423K for 12 hours under vacuum before measurements and then recorded at 77K.

X-ray diffraction (XRD) patterns of the fresh catalysts were obtained on a SIEMENS D6000 instrument in the range of 1.5-70° with a scanning step of 0.02 using CuKα radiation (0.1542nm wavelength). A high resolution scanning electron microscope (SEM) (LEO 1530) was used to obtain the surface morphology of the fresh and reacted catalyst. Transmission electron microscopy (TEM) (Philips CM200) was used to characterize and examine the fresh catalysts.

Temperature-programmed oxidation (TPO) of the reacted catalysts was utilized to obtain the degree of coke deposition by using a Stanton-Redcroft thermogravimetric analyser (TGA and DTG). About 10 mg of the reacted catalyst was heated in air at 15 ^oC min^{-1} to a final temperature of 800 ^oC, with a dwell time of 10 min. Temperature programmed reduction (TPR) of the prepared catalysts were carried out using a modified thermogravimetric analyzer (SDTQ600) coupled with a mass spectrometer (ThermoStar GSD301). Prior to the commencement of TPR, the sample was heated at 20 ^oC min^{-1} in pure N_2 (500 ml min^{-1}) from room temperature to 500 ^oC. The pre-treated catalysts were cooled to room temperature before heating to 1000 ^oC at a rate of 10 ^oC min^{-1} in a H_2 atmosphere. During the reduction process, variance of generated gas and mass loss were respectively monitored by MS and TGA through a heated capillary delivery.

NH_3-TPD was performed on Chem BET TPR/TPD Chemisorption Analyzer, CBT-1, QuantaChrome instruments. Typically, 30 mg of the samples were pretreated at 500 ^oC for 1h in He flow at a flow rate of 120 ml min^{-1} to purge the gas or moisture adsorbed on the samples, then the temperature was cooled to adsorption temperature of 100 ^oC, followed by adsorption of the gas mixture of NH_3 and He (8.16%, mol/mol) for 30min or 15min,

respectively. After adsorption, pure He flow (120ml min^{-1}) was passed through the samples which were heated from 100 to 1100 ^{o}C at a heating rate of 10 ^{o}C min^{-1}.

3. Results and discussion

3.1 Characterization of fresh catalysts

The same type of mesoporous silica material MCM-41 has been prepared and impregnated with Ni particles as described in the above experimental section. Their XRD patterns have been listed in Figures 1 and 2. As shown in the XRD patterns of the small angle region (2θ = 1.5-10°), all Nicatalysts expressed a typical pattern of MCM-41 material with a hexagonal framework of strong (100) reflection at 2-2.5°. The weak (110) and (200) reflections at 4.3° and 4.9° have been clearly observed for Ni catalysts on H-[Si]MCM-41 support, which illustrate the long-range order of MCM-41 materials [47]. However, for Na-[Si]MCM-41 and H-[Al]MCM-41supports, (110) and (200) reflections were small and difficult to be detected in Figure 1 due to the disturbance of the long-range order after introducing Na and Al [48, 49].

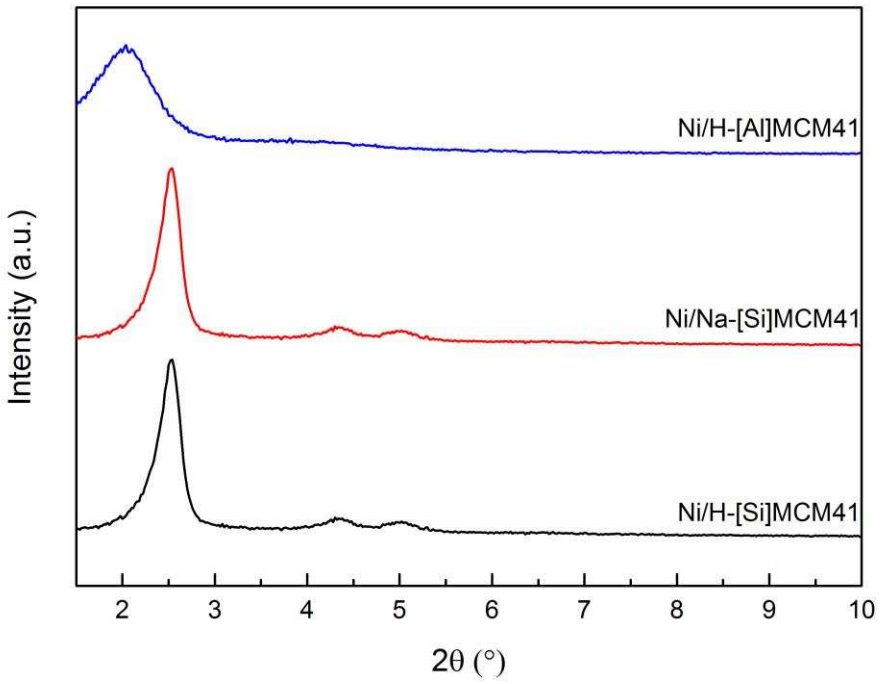

Figure 1: Small angel XRD pattern of Ni catalysts on Ni/H-[Al] MCM-41, Ni/Na-[Si] MCM-41 and Ni/H-[Si] MCM-41 supports.

For the XRD patterns for Ni/MCM-41 catalysts in the range of 2θ between 10-70°, a broad amorphous silica peak has been detected at around 23° as shown in Figure 2. No strong and sharp peaks have been observed for the existence of well crystalline NiO particles. Only three broad and weak diffraction peaks were detected at 37 º, 43 º and 64 º, corresponding to very fine NiO nanoparticles with NiO (101), NiO (012) and NiO (110), respectively. The particle size was estimated to be around 3 nm for all catalysts according to the Scherrer's formula for the width of the half intensity peak. These very fine NiO nano-particles were probably located inside nano-pores of MCM-41support instead of staying on the surface.

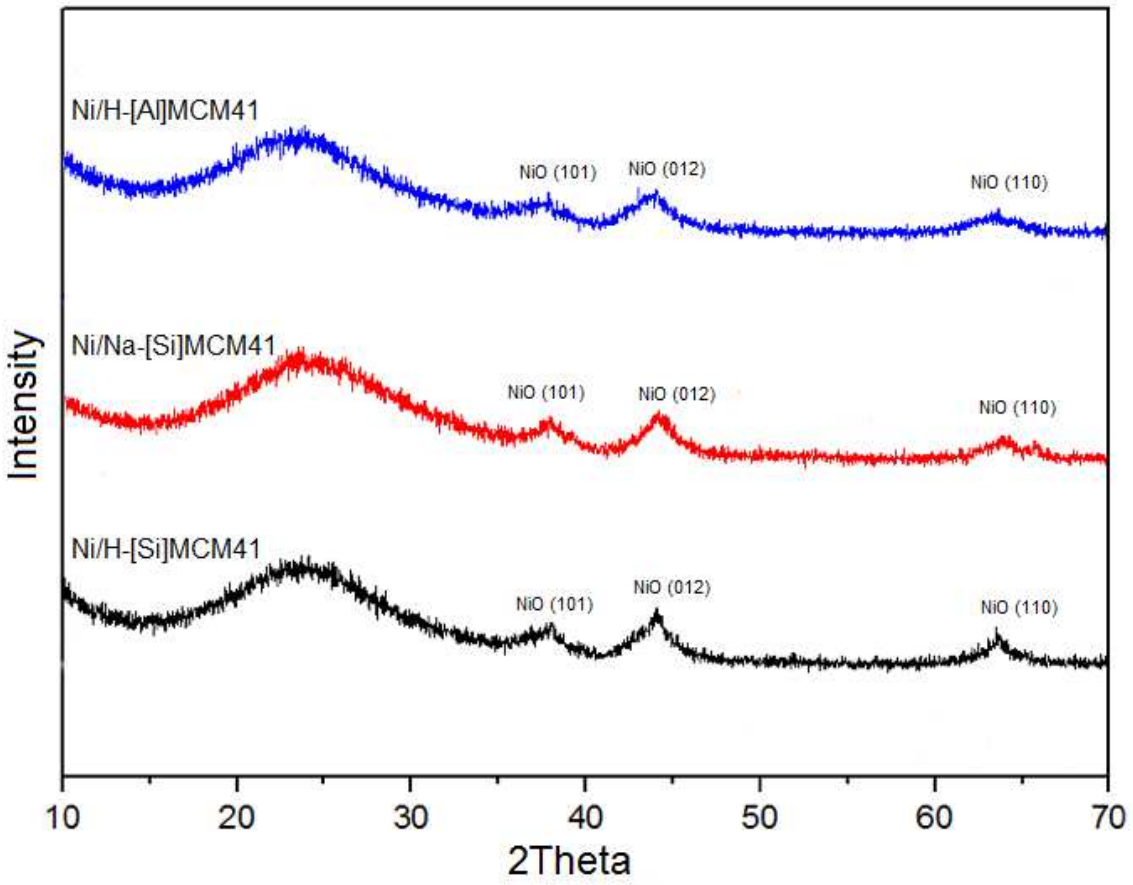

Figure 2: XRD analysis of Ni/MCM-41 catalysts

The N_2 adsorption-desorption isotherms and corresponding Barrett-Joyner-Halenda (BJH) pore size distribution curves are presented in Figure 3 (a) and (b), respectively. All Ni/MCM-41 catalysts showed type IV isotherms, indicating a mesoporous structure

according to the IUPAC classification. The pore size distribution was evaluated by the BJH model, which corresponds to narrow and uniform mesopores around 2-3 nm for all Ni/MCM-41 catalysts. The BET surface areas, total pore volumes, and average pore diameters have been determined by N_2 adsorption and desorption isotherms and summarized in Table 1. Ni/MCM-41 catalysts showed a high surface area around 800-1000 $m^2\ g^{-1}$. The Ni/H-[Si]MCM-41 demonstrates the highest surface area (1018.677 $m^2\ g^{-1}$), which was followed by the Ni/Na-[Si]MCM-41 (1012.769 $m^2\ g^{-1}$), and Ni/H-[Al] MCM-41 (800.237 $m^2\ g^{-1}$), due to the disturbance of the long-range order after introducing Na and Al as detected by the above XRD investigation. The average pore diameter was between 2 and 3 nm with the total pore volume changing from 0.593 to 0.825 $cm^3\ g^{-1}$.

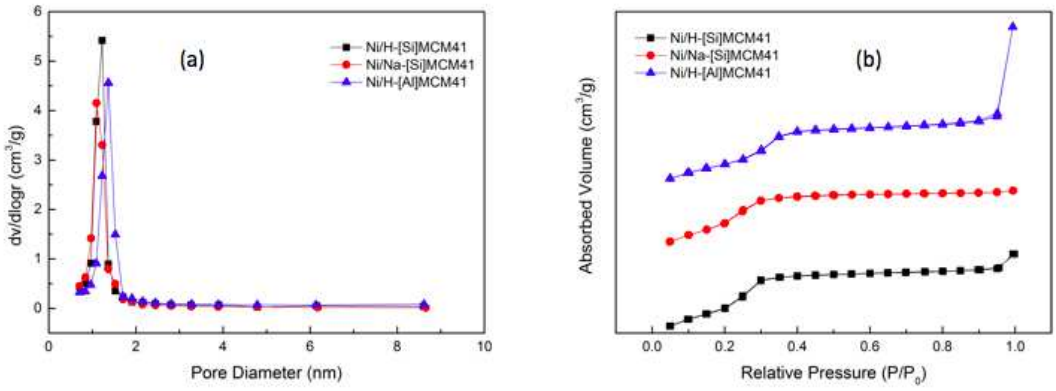

Figure 3: Pore size distribution (a) and N_2 adsorption/desorption isotherms of the fresh catalyst (b)

Table 1: Surface areas, pore volumes, and pore diameters of Ni/MCM-41 catalysts

Sample	Surface area [a] (m^2/g)	Total pore volume [a] (cm^3/g)	Average Pore diameter [a] (nm)
Ni/H-[Si]MCM41	1018.677	0.746	2.92
Ni/H-[Al]MCM41	800.237	0.825	3.12
Ni/Na-[Si]MCM41	1012.769	0.593	2.34

[a] Surface area pore volume and average pore diameter calculated from N_2 adsorption/desorption isotherms

SEM and TEM investigations have also been carried out for the characterization of the Ni/MCM-41 catalysts. NiO crystal (normally ca. 200 nm on silica or alumina surface) had not been obviously detected on the outside surface of mesoporous supports Ni/H-[Al]MCM-41, Ni/Na-[Si]MCM-41and Ni/H-[Si]MCM-41, as shown in the SEM images in Figure 4. The impregnated NiO particles were probably located inside the nano-pores of MCM-41 supports. The Ni/Na-[Si]MCM-41and Ni/H-[Si]MCM-41showed the similar shape and size of MCM-41 particles. However, the support particles were very fine on Ni/H-[Al]MCM-41 after introduction of Al during the preparation. The disturbance of the long-range order after introducing Al might break the growing of MCM-41 particles during the synthesis and caused the very fine particles.

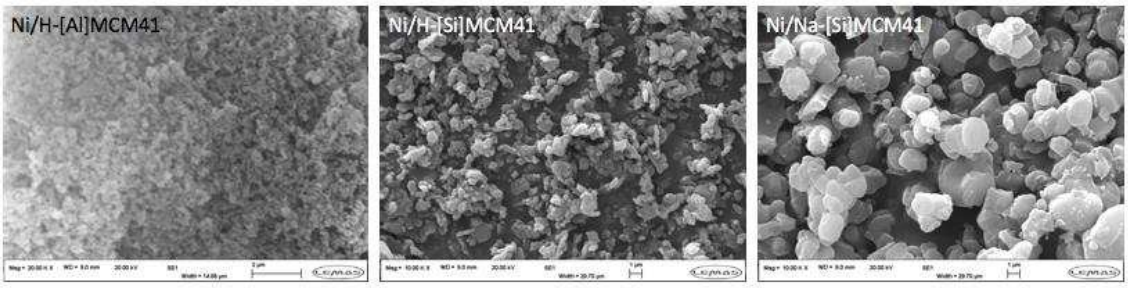

Figure 4: SEM images of Ni/MCM-41 catalysts

TEM images confirmed that the long-range order of the MCM-41 structure of H-[Si]MCM-41 as indicated by the XRD pattern and the uniform mesopores have been clearly observed in Figure 5. The long-range order of MCM-41 mesoporous structure has been slightly disturbed after indroducing Na during the synthesis and strongly disturbed by the introduction of Al as shown in Figure 5, which is consistent with the XRD results. The NiO particles have been homogeneously dispersed inside the nanopores of all MCM-41 supports with the main particle size around 2-3 nm as proven by TEM analysis in Figure 5. No large Ni crystals have been observed on the surface of the Ni/H-[Al]MCM-41, Ni/H-

[Si]MCM-41 and Ni/Na-[Si]MCM-41 catalysts as indicated by both TEM and SEM images, similar as the XRD patterns.

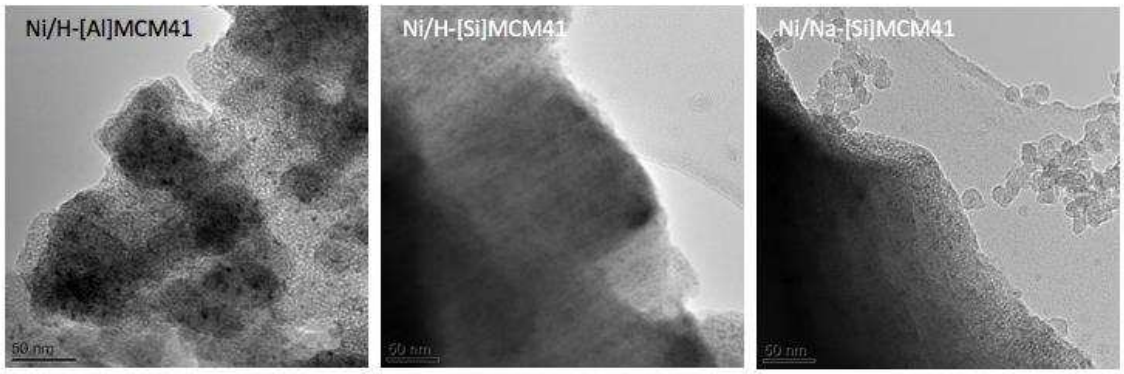

Figure 5: TEM images of Ni/MCM-41 catalysts

The reduction property and surface NiO species of the Ni/MCM-41 catalysts have been carried out by TPR investigation and their curves are shown in Figure 6. The small reduction peak around 390 ^{o}C has been only observed for the Ni/Na-[Si]MCM-41 and the Ni/H-[Si]MCM-41 catalysts, which could be caused by the reduction of Ni nanoparticles on the outside surface of MCM-41 supports [39].The strong and large peak at the higher reduction temperature around 660-700 ^{o}C occurred on all Ni/MCM-41 catalysts, which was assigned to the very fine NiO nanoparticles inside the nanopores of MCM-41 supports (2-3 nm) [40]. It was reported that smaller metal oxide nanoparticles required higher temperature for hydrogen reduction with the stronger interaction between metal and supports [41, 42]. Obviously, most NiO particles were very fine nanoparticles around 2-3 nm and small enough inside pores of MCM-41 supports. In addition, compared to the Ni/Na-[Si]MCM-41 and the Ni/H-[Si]MCM-41, the reduction peak at high temperature shifted slightly to the lower temperature on the Ni/H-[Al]MCM-41, which indicated the Al addition and the generation of surface acidity enhanced the reducibility of NiO nanoparticles.

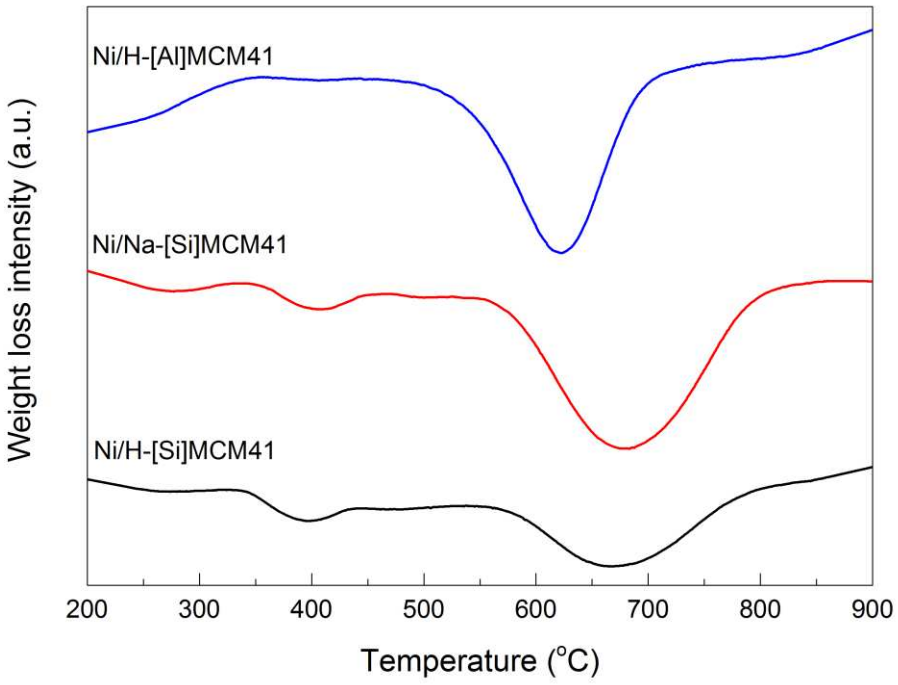

Figure 6: TPR analysis of Ni/MCM-41 catalysts

The surface acidity of the catalysts has been probed by the chem-adsorption/desorption of basic molecule ammonia via NH_3-TPD, a popular method utilized to analyze the acidity of catalysts. As shown in Figure 7, a strong and broad desorption peak has been observed at 200 to 400 ^oC for the Ni/H-[Al] MCM-41 due to the formation of large amount of surface acid sites after introducing Al into the silica network. The 4-charged Si cation replaced by the 3-charged Al cation would induce a native charged O (O^-) site and require a proton on network O^-, which could generate surface SiOHAl groups as Brϕnsted acid sites (Al species incorporated into silica network near SiOH groups) [35-38]. Only a very weak and broad desorption temperature peak was observed at 200-300 ^oC for the Ni/H-[Si]MCM-41, which indicated the presence of most of neutral sites (SiOH groups) on the surface with a very small amount of weak acidic Q^3 SiOH groups. No obvious peak has been detected for the Ni/Na-[Si]MCM-41, which indicated that the Na-[Si]MCM-41 support did not offer the surface acid sites and acidic Q^3 SiOHs have been totally replaced by Na cations. .

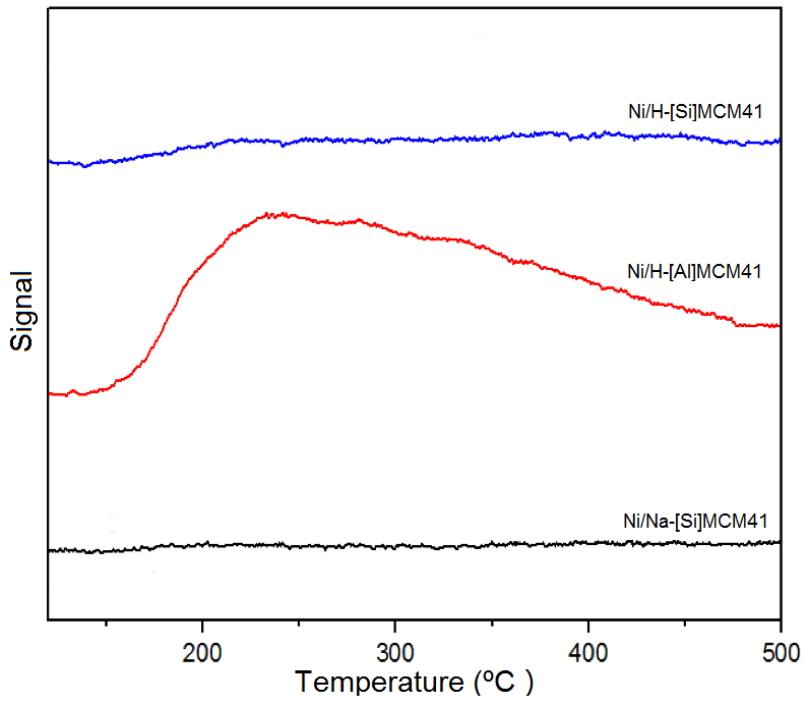

Figure 7: NH_3-TPD of Ni/MCM-41 catalysts

3.2. The pyrolysis/gasification of wood sawdust on Ni/MCM-41 catalysts

The pyrolysis/gasification of wood sawdust was carried out on Ni/MCM-41 catalysts in a two stage reactor system. Gas yield, mass balance, and gas compositions of CO, H_2, CO_2, CH_4 and C_2-C_4 hydrocarbons during the gasification of wood sawdust are presented in Table 2 and Figure 8.

For all the Ni/MCM-41 catalysts, most of Ni particles were located inside nanopores with a uniform size of 2-3 nm. The biomass gasification is suggested to be derived via the Ni active centers. Therefore, similar Ni particles should offer similar activity. However, a different catalytic performance has been clearly observed during the pyrolysis/gasification on Ni/MCM-41 catalysts with various surface acidity. Clearly, the support acidity has influenced the biomass gasification on supported Ni catalysts. As shown in Table 2, the Ni/Na-[Si]MCM-41catalyst without surface acidity showed the lowest gas yield and hydrogen yield during the gasification. The Ni/H-[Si]MCM-41catalyst with the small amount of weak acidic SiOH groups contributed the higher gas yield compared to that of the Ni/H-[Al]MCM-41 with a large amount of Brϕnsted acid sites. The significant

amount of Brϕnsted acid sites on the surface of supports could not cause the higher gasification rates. The well hexagonal structure of MCM-41 supports might result in the better diffusion of pyrolysis chemical vapor inside the pores of Ni/H-[Si]MCM-41catalyst resulting in a higher gasification rate.

Table 2: Mass balance and gas compositions from the gasification on Ni/MCM-41 catalysts

Catalyst bed	Ni/H-[Al] MCM41	Ni-H-[Si] MCM41	Ni/Na-[Si] MCM41
Gas/wood (wt. %)*	63.9	73.6	51.8
Mass balance (wt. %)*	94.72	101.35	95.63
H_2 yield (mmol H_2 g^{-1} sample)	21.6	9.8	6.7

*The gas, residue yields and mass balance presented in was calculated via the following equations:

$$\text{Gas yield (wt. \%)} = \frac{\text{Gas mass}}{\text{wood sawdust mass}} \times 100$$

$$\text{Mass balance (wt. \%)} = \frac{\text{Gas mass+Liquid mass+Char mass+Residue mass}}{\text{Wood sawdust mass+injected water mass}} \times 100$$

However, the hydrogen production has been significantly improved for the reaction on the Ni/H-[Al]MCM-41 catalyst with a large amount of Brϕnsted acid sites. The hydrogen yield on the Ni/H-[Al]MCM-41 (21.6 mmol H_2 g^{-1} sample) was more than two to three times higher than that on the other two Ni/MCM-41 catalysts (6.7 and 9.8 mmol H_2 g^{-1} sample). The Ni/H-[Si]MCM-41 catalyst with only a small amount of weak acidic SiOH groups contributed a slightly higher hydrogen yield than that produced from no acidic Ni/Na-[Si]MCM-41 catalyst. Obviously, the large amount of Brϕnsted acid sites on the support surface could not enhance the gasification rate as detected before, but significantly improved the reforming for hydrogen production. Lliopoulou et al [45] reported that the enhancement of surface acidity of H-[Al]MCM-41 catalysts could promote the hydrocarbon conversion and cracking for the upgrading of biomass pyrolysis oils. Therefore, the Ni/H-[Al]MCM-41 worked as a bifunctional catalyst and the large amount of Brϕnsted acid sites was proposed to transfer the pyrolysis derived chemicals into smaller

compounds for more efficient reforming on the Ni surface. In addition, compared with the similar reduction peaks for the Ni/H-[Si]MCM-41and the Ni/Na-[Si]MCM-41 catalysts, the Ni/H-[Al]MCM-41demonstrated a relatively lower temperature and sharp reduction peak in the TPR analysis, indicating the different Ni surface property on the Ni/H-[Al]MCM-41 compared to the other two Ni/MCM-41 catalysts and influencing their reforming performance.

As shown in Figure 8, the fraction of the gas composition also confirmed that the reforming process has been strongly enhanced on the Ni/H-[Al]MCM-41. The Ni/H-[Si]MCM-41 catalyst showed the slightly enhanced reforming performance than the Ni/Na-[Si]MCM-41 catalyst, however, both catalysts produced a significant amount of CH_4 (ca. 30 Vol.%) with a small amount of C_2-C_4 hydrocarbons (ca. 5 Vol.%). These hydrocarbon compounds almost disappeared using the Ni/H-[Al]MCM-41 catalyst. The CO_2 gas fraction was higher with the Ni/H-[Al]MCM-41, suggesting that the dry reforming of hydrocarbons with CO_2 was not promoted by the Ni catalysts on acidic supports. It was consistent with the literature[21] that incorporating Al to the MCM-41 framework did not promote methane dry reforming on Ni catalysts. Therefore, the steam reforming of hydrocarbons was proposed to significantly improve the hydrogen production on the Ni/H-[Al]MCM-41 catalyst (increased from ca. 25 Vol.% up to ca. 55 Vol.%). For the steam reforming of hydrocarbons, CO should be produced and the CO fraction should be increased. However, the Ni/H-[Al]MCM-41 catalyst contributed the lowest CO fraction compared to the other two catalysts, indicating the existence of the water gas shift reaction and the consumption of CO to further increase hydrogen production as also reported by previous papers in the steam reforming of hydrocarbons [4, 43, 44].

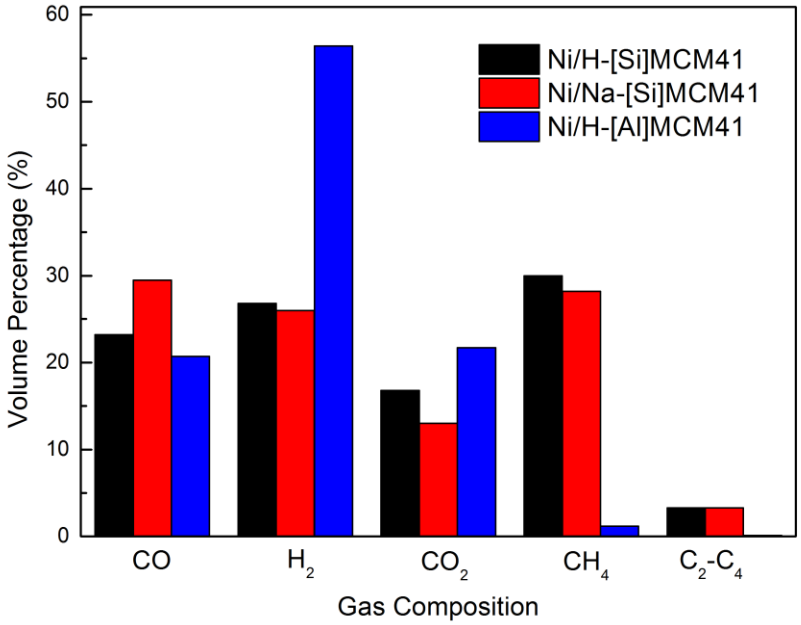

Figure 1 Gas composition from biomass gasification

The reacted catalysts were analyzed by temperature programmed oxidation (TPO) to determine the amount and type of deposited coke. Oxidation of carbon occurred after 550℃, which was assigned to filamentous type carbons formed during the gasification process [48, 49]. As shown in Figure 9, low coke deposition has been detected for the Ni/MCM-41 catalysts. The coke deposition was 1.8 wt%, 1.6 wt%, and 1.3 wt% on the Ni/H-[Al]MCM-41, Ni/H-[Si]MCM-41, and Ni/Na-[Si]MCM-41 catalysts, respectively. It has been widely reported that highly active catalysts in gasification or reforming would cause high coke deposition.

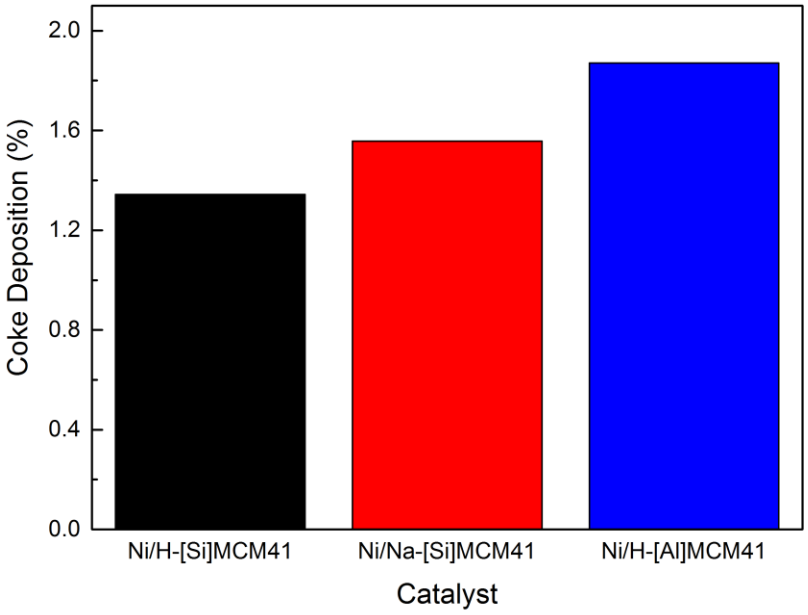

Figure 9: Weight ratios of coke to the catalyst for the Ni/MCM-41catalysts after the gasification

As shown in Figure 10, the deposited coke was hard to be observed on the outside surface of the MCM-41 catalysts as shown in their SEM images. The small amount of filamentous carbon confirmed by TPO might be located on the Ni surface inside pores of MCM-41. The reacted Ni/MCM-41 catalysts were analyzed by XRD to confirm whether the sintering occurred for the Ni particles. As shown in Figure 11, the XRD patterns did not show any obvious change for the Ni/MCM-41 catalysts before and after reaction, indicating almost no sintering during the gasification process. Only small new diffraction peaks at 44 and 52° were observed due to the generation of Ni particles after the gasification of sawdust [53]. It was reported that the NiO was reduced to Ni during the gasification process under the reducing environment. Therefore, an easier and safer process was carried out without the pre-reduction with H_2 during the catalyst process. Therefore, Ni/MCM-41 catalysts were quite stable for biomass gasification.

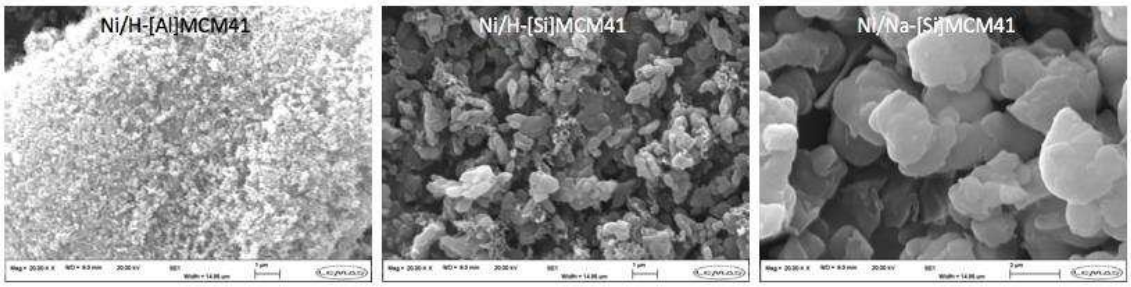

Figure 10: SEM analysis of reacted catalysts

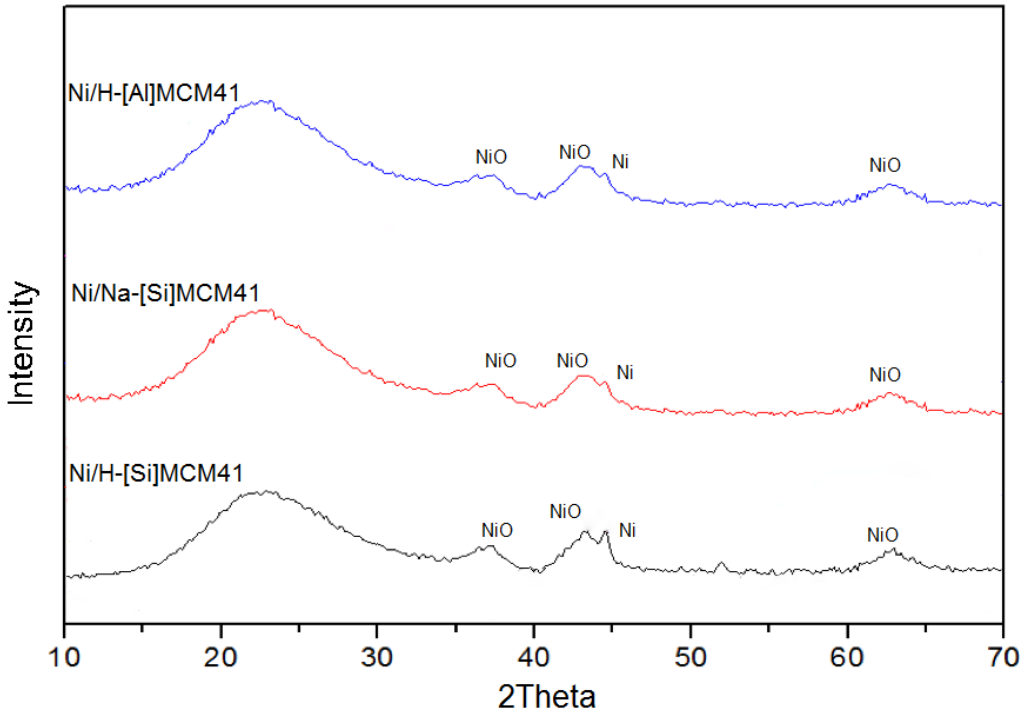

Figure 11: XRD analysis of reacted catalysts

4. Conclusions

In this work, the obtained Ni/MCM-41catalysts with and without support acidity were investigated for hydrogen production from the biomass gasification of wood sawdust. MCM-41 supports were synthesized with acidity (Al form Ni/H-[Al] MCM-41), without acidity (neutral form Ni/H-[Si]MCM-41, may exist as very weak acidic surface SiOH groups), and without acidity (Na form Ni/Na-[Si]MCM-41). The Ni/H-[Si]MCM-41 catalyst demonstrated the highest surface area (1018.677 m^2/g), which was followed by

Ni/Na-[Si]MCM-41 (1012.769 m^2/g), and the Ni/H-[Al] MCM-41 (800.237 m^2/g), due to the disturbance of the long-range order after introducing Na and Al as detected by XRD investigation. As expected, a large amount of surface acid sites have been generated after introducing Al into the silica network near SiOH groups on the Ni/H-[Al] MCM-41. Most of neutral sites (SiOH groups) on the surface with very a small amount of weak acidic Q^3 SiOH groups were formed on the Ni/H-[Si]MCM-41 catalyst. No acidity was observed for the Ni/Na-[Si]MCM-41. Most of Ni nanoparticles had a similar size at 2-3 nm and were located inside the nanopores of MCM-41 supports, which could minimize the effects from the Ni particle size for the biomass gasification. Compared to the Ni/Na-[Si]MCM-41 and the Ni/H-[Si]MCM-41 catalysts, the reduction peak at high temperature shifted slightly to the lower temperature on the Ni/H-[Al]MCM-41 catalyst, which indicated the Al addition and the generation of surface acidity enhanced the reducibility of NiO nanoparticles.

The large amount of Brϕnsted acid sites on the Ni/H-[Al]MCM-41 catalyst could not cause the higher gasification rates, and the Ni/H-[Si]MCM-41catalyst with the small amount of weak acidic SiOH groups contributed the highest gas yield. In addition, the presence of significant Brϕnsted acid sites promoted the conversion of hydrocabrons derived from biomass pyrolysis into smaller molecular products including H_2 and CO. However, the large amount of Brϕnsted acid sites on the supports has significantly improved the reforming and hydrogen production during the wood sawdust gasification. The hydrogen yield on the Ni/H-[Al]MCM-41 (21.6 mmol H_2 g^{-1} sample) was more than two to three times higher than that on the other two Ni/MCM-41 catalysts (6.7 and 9.8 mmol H_2 g^{-1} sample). The surface acid sites helpped crack and transfer the pyrolysis chemicals into smaller compounds for the more efficient reforming on the Ni surface inside nanopores. Low coke deposition has been detected for Ni/MCM-41 catalysts (less than 2 wt% of filamentous type carbons on the Ni/H-[Al]MCM-41, Ni/H-[Si]MCM-41, and Ni/Na-[Si]MCM-41 catalysts), corresponding to their activity in gasification. The obtained Ni/MCM-41 catalysts were quite stable and almost no sintering has been observed after gasification at 800 ^oC.

Acknowledgement

This work was supported by the International Exchange Scheme from the Royal Society (IE110273), UK, the Australian Research Council DP150103842, and the Early Career Research Scheme and MCR from the University of Sydney.

References

[1] B.C.R. Ewan, R.W.K. Allen, A figure of merit assessment of the routes to hydrogen, International Journal of Hydrogen Energy, 30 (2005) 809-819.
[2] A.F. Kirkels, G.P.J. Verbong, Biomass gasification: Still promising? A 30-year global overview, Renewable and Sustainable Energy Reviews, 15 (2011) 471-481.
[3] C. Wu, P.T. Williams, Hydrogen production by steam gasification of polypropylene with various nickel catalysts, Applied Catalysis B: Environmental, 87 (2009) 152-161.
[4] C. Wu, Z. Wang, J. Huang, P.T. Williams, Pyrolysis/gasification of cellulose, hemicellulose and lignin for hydrogen production in the presence of various nickel-based catalysts, Fuel, 106 (2013) 697-706.
[5] Y. Richardson, J. Blin, G. Volle, J. Motuzas, A. Julbe, In situ generation of Ni metal nanoparticles as catalyst for H2-rich syngas production from biomass gasification, Applied Catalysis A: General, 382 (2010) 220-230.
[6] M. Ni, D.Y.C. Leung, M.K.H. Leung, A review on reforming bio-ethanol for hydrogen production, International Journal of Hydrogen Energy, 32 (2007) 3238-3247.
[7] I. Luisetto, S. Tuti, C. Battocchio, S. Lo Mastro, A. Sodo, Ni/CeO2–Al2O3 catalysts for the dry reforming of methane: The effect of CeAlO3 content and nickel crystallite size on catalytic activity and coke resistance, Applied Catalysis A: General, 500 (2015) 12-22.
[8] D. Baudouin, U. Rodemerck, F. Krumeich, A.d. Mallmann, K.C. Szeto, H. Ménard, L. Veyre, J.-P. Candy, P.B. Webb, C. Thieuleux, C. Copéret, Particle size effect in the low temperature reforming of methane by carbon dioxide on silica-supported Ni nanoparticles, Journal of Catalysis, 297 (2013) 27-34.
[9] S. Zhang, S. Muratsugu, N. Ishiguro, M. Tada, Ceria-Doped Ni/SBA-16 Catalysts for Dry Reforming of Methane, ACS Catalysis, 3 (2013) 1855-1864.
[10] D. Baudouin, U. Rodemerck, F. Krumeich, A.d. Mallmann, K.C. Szeto, H. Ménard, L. Veyre, J.-P. Candy, P.B. Webb, C. Thieuleux, C. Copéret, Particle size effect in the low

temperature reforming of methane by carbon dioxide on silica-supported Ni nanoparticles, Journal of Catalysis, 297 (2013) 27-34.
[11] A.L.M. da Silva, J.P. den Breejen, L.V. Mattos, J.H. Bitter, K.P. de Jong, F.B. Noronha, Cobalt particle size effects on catalytic performance for ethanol steam reforming – Smaller is better, Journal of Catalysis, 318 (2014) 67-74.
[12] C. Wu, L. Dong, J. Onwudili, P.T. Williams, J. Huang, Effect of Ni Particle Location within the Mesoporous MCM-41 Support for Hydrogen Production from the Catalytic Gasification of Biomass, ACS Sustainable Chemistry & Engineering, 1 (2013) 1083-1091.
[13] H. Liang, Y. Zhang, Y. Liu, Three-dimensionally ordered macro-porous Pt/TiO2 catalyst used for water-gas shift reaction, Journal of Natural Gas Chemistry, 17 (2008) 403-408.
[14] Y. Zhang, H. Liang, X.Y. Gao, Y. Liu, Three-dimensionally ordered macro-porous CuO–CeO2 used for preferential oxidation of carbon monoxide in hydrogen-rich gases, Catalysis Communications, 10 (2009) 1432-1436.
[15] Y.e. Zheng, X. Zhu, H. Wang, K. Li, Y. Wang, Y. Wei, Characteristic of macroporous CeO2-ZrO2 oxygen carrier for chemical-looping steam methane reforming, Journal of Rare Earths, 32 (2014) 842-848.
[16] M.E. Gálvez, A. Albarazi, P. Da Costa, Enhanced catalytic stability through non-conventional synthesis of Ni/SBA-15 for methane dry reforming at low temperatures, Applied Catalysis A: General, 504 (2015) 143-150.
[17] D. Li, L. Zeng, X. Li, X. Wang, H. Ma, S. Assabumrungrat, J. Gong, Ceria-promoted Ni/SBA-15 catalysts for ethanol steam reforming with enhanced activity and resistance to deactivation, Applied Catalysis B: Environmental, 176–177 (2015) 532-541.
[18] Z.A. Alothman, A Review: Fundamental Aspects of Silicate Mesoporous Materials, Materials, 5 (2012) 2874-2902.
[19] R. Huirache-Acuna, R. Nava, C.L. Peza-Ledesma, J. Lara-Romero, G. Alonso-Nunez, B. Pawelec, E.M. Rivera-Munoz, SBA-15 Mesoporous Silica as Catalytic Support for Hydrodesulfurization Catalysts-Review, Materials, 6 (2013) 4139-4167.
[20] M.H. Youn, J.G. Seo, H. Lee, Y. Bang, J.S. Chung, I.K. Song, Hydrogen production by auto-thermal reforming of ethanol over nickel catalysts supported on metal oxides: Effect of support acidity, Applied Catalysis B: Environmental, 98 (2010) 57-64.

[21] E. Lovell, Y. Jiang, J. Scott, F. Wang, Y. Suhardja, M. Chen, J. Huang, R. Amal, CO2 reforming of methane over MCM-41-supported nickel catalysts: altering support acidity by one-pot synthesis at room temperature, Applied Catalysis A: General, 473 (2014) 51-58.
[22] M.C. Sánchez-Sánchez, R.M. Navarro, J.L.G. Fierro, Ethanol steam reforming over Ni / Mx Oy-Al2 O3 (M = Ce, La, Zr and Mg) catalysts: Influence of support on the hydrogen production, International Journal of Hydrogen Energy, 32 (2007) 1462-1471.
[23] M.H. Youn, J.G. Seo, K.M. Cho, J.C. Jung, H. Kim, K.W. La, D.R. Park, S. Park, S.H. Lee, I.K. Song, Effect of support on hydrogen production by auto-thermal reforming of ethanol over supported nickel catalysts, Korean Journal of Chemical Engineering, 25 (2008) 236-238.
[24] Y. Yang, J. Ma, F. Wu, Production of hydrogen by steam reforming of ethanol over a Ni/ZnO catalyst, International Journal of Hydrogen Energy, 31 (2006) 877-882.
[25] J. Zhang, J. Chen, J. Ren, Y. Li, Y. Sun, Support effect of Co/Al2O3 catalysts for Fischer-Tropsch synthesis, Fuel, 82 (2003) 581-586.
[26] E.G. Baker, L.K. Mudge, M.D. Brown, Steam gasification of biomass with nickel secondary catalysts, Industrial & Engineering Chemistry Research, 26 (1987) 1335-1339.
[27] K.N. Tayade, M. Mishra, Catalytic activity of MCM-41 and Al grafted MCM-41 for oxidative self and cross coupling of amines, Journal of Molecular Catalysis a-Chemical, 382 (2014) 114-125.
[28] X. Li, A.J. Wang, S. Zhang, Y.Y. Chen, Y.K. Hu, Effect of surface Na+ or K+ ion exchange on hydrodesulfurization performance of MCM-41-supported Ni-W catalysts, Applied Catalysis a-General, 316 (2007) 134-141.
[29] C.-F. Cheng, J. Klinowski, Synthesis and characterization of the mesoporous galloaluminosilicate molecular sieve MCM-41, Journal of the Chemical Society, Faraday Transactions, 92 (1996) 289-292.
[30] F. Chen, C. Wu, L. Dong, A. Vassallo, P.T. Williams, J. Huang, Characteristics and catalytic properties of Ni/CaAlOx catalyst for hydrogen-enriched syngas production from pyrolysis-steam reforming of biomass sawdust, Applied Catalysis B: Environmental, 183 (2016) 168-175.
[31] Z. Wang, Y. Jiang, R. Rachwalik, Z. Liu, J. Shi, M. Hunger, J. Huang, One-Step Room-

Temperature Synthesis of [Al]MCM-41 Materials for the Catalytic Conversion of Phenylglyoxal to Ethylmandelate, ChemCatChem, 5 (2013) 3889-3896.
[32] N.T. Mathew, S. Khaire, S. Mayadevi, R. Jha, S. Sivasanker, Rearrangement of allyl phenyl ether over Al-MCM-41, Journal of Catalysis, 229 (2005) 105-113.
[33] X. Chen, L. Huang, G. Ding, Q. Li, Characterization and catalytic performance of mesoporous molecular sieves Al-MCM-41 materials, Catalysis Letters, 44 (1997) 123-128.
[34] L. Alvarado Perea, T. Wolff, P. Veit, L. Hilfert, F.T. Edelmann, C. Hamel, A. Seidel-Morgenstern, Alumino-mesostructured Ni catalysts for the direct conversion of ethene to propene, Journal of Catalysis, 305 (2013) 154-168.
[35] A. Corma, V. Fornes, M.T. Navarro, J. Perezpariente, Acidity and Stability of MCM-41 Crystalline Aluminosilicates, Journal of Catalysis, 148 (1994) 569-574.
[36] M. Hartmann, A. Pöppl, L. Kevan, Ethylene dimerization and butene isomerization in nickel-containing MCM-41 and AlMCM-41 mesoporous molecular sieves: An electron spin resonance and gas chromatography study, Journal of Physical Chemistry, 100 (1996) 9906-9910.
[37] H. Kosslick, G. Lischke, G. Walther, W. Storek, A. Martin, R. Fricke, Physico-chemical and catalytic properties of Al-, Ga- and Fe-substituted mesoporous materials related to MCM-41, Microporous Materials, 9 (1997) 13-33.
[38] H. Kosslick, G. Lischke, B. Parlitz, W. Storek, R. Fricke, Acidity and active sites of Al-MCM-41, Applied Catalysis A: General, 184 (1999) 49-60.
[39] W.S. Dong, H.S. Roh, K.W. Jun, S.E. Park, Y.S. Oh, Methane reforming over Ni/Ce-ZrO2 catalysts: Effect of nickel content, Applied Catalysis A: General, 226 (2002) 63-72.
[40] A.M. Diskin, R.H. Cunningham, R.M. Ormerod, The oxidative chemistry of methane over supported nickel catalysts, Catalysis Today, 46 (1998) 147-154.
[41] A.Y. Khodakov, J. Lynch, D. Bazin, B. Rebours, N. Zanier, B. Moisson, P. Chaumette, Reducibility of Cobalt Species in Silica-Supported Fischer–Tropsch Catalysts, Journal of Catalysis, 168 (1997) 16-25.
[42] R. Bechara, D. Balloy, J.-Y. Dauphin, J. Grimblot, Influence of the Characteristics of γ-Aluminas on the Dispersion and the Reducibility of Supported Cobalt Catalysts, Chemistry of Materials, 11 (1999) 1703-1711.
[43] A. Demirbaş, Mechanisms of liquefaction and pyrolysis reactions of biomass, Energy

Conversion and Management, 41 (2000) 633-646.
[44] A.K. Avetisov, J.R. Rostrup-Nielsen, V.L. Kuchaev, J.H. Bak Hansen, A.G. Zyskin, E.N. Shapatina, Steady-state kinetics and mechanism of methane reforming with steam and carbon dioxide over Ni catalyst, Journal of Molecular Catalysis A: Chemical, 315 (2010) 155-162.
[45] E.F. Iliopoulou, E.V. Antonakou, S.A. Karakoulia, I.A. Vasalos, A.A. Lappas, K.S. Triantafyllidis, Catalytic conversion of biomass pyrolysis products by mesoporous materials: Effect of steam stability and acidity of Al-MCM-41 catalysts, Chemical Engineering Journal, 134 (2007) 51-57.
[46] C. Wu, P.T. Williams, Investigation of Ni-Al, Ni-Mg-Al and Ni-Cu-Al catalyst for hydrogen production from pyrolysis–gasification of polypropylene, Applied Catalysis B: Environmental, 90 (2009) 147-156.
[47] J. Chen, X. Li, Y. Li, Y. Qin, Production of hydrogen and nanocarbon from direct decomposition of undiluted methane on high-nickeled Ni-Cu-alumina catalysts, Chemistry Letters, 32 (2003) 424-425.
[48] S.-Y. Wang, M.-J. Tsai, Assessment of temperature and relative humidity conditioning performances of interior decoration materials, J Wood Sci, 44 (1998) 267-274.
[49] S. Wang, A Comprehensive Study on Carbon Dioxide Reforming of Methane over Ni/γ-Al2O3 Catalysts, Industrial & Engineering Chemistry Research, 38 (1999) 2615-2625.
[50] P.H. Blanco, C. Wu, J.A. Onwudili, P.T. Williams, Characterization and evaluation of Ni/SiO2 catalysts for hydrogen production and tar reduction from catalytic steam pyrolysis-reforming of refuse derived fuel, Applied Catalysis B: Environmental, 134–135 (2013) 238-250.
[51] P.H. Blanco, C. Wu, P.T. Williams, Influence of Ni/SiO2 catalyst preparation methods on hydrogen production from the pyrolysis/reforming of refuse derived fuel, International Journal of Hydrogen Energy, 39 (2014) 5723-5732.
[52] C. Wu, P.T. Williams, A Novel Nano-Ni/SiO2 Catalyst for Hydrogen Production from Steam Reforming of Ethanol, Environmental Science & Technology, 44 (2010) 5993-5998.
[53] C. Wu, P.T. Williams, Investigation of coke formation on Ni-Mg-Al catalyst for hydrogen production from the catalytic steam pyrolysis-gasification of polypropylene, Applied Catalysis B: Environmental, 96 (2010) 198-207.